Hollow core/shell beta-Bi_2O_3@WS_2 p-n heterojunction for efficient photocatalytic degradation of fluoroquinolones: a theoretical and experimental study

Li Li [a], Yunhui Yan [c], Haiping Liu [a], Jinge Du [a], Shuai Fu [a], Fengying Zhao [a], Si-Min Xu [d,*], Jianguo Zhou [a,b,*]

[a] *School of Environment, Key Laboratory of Yellow River and Huai River Water Environment and Pollution Control (Ministry of Education), Henan Engineering Laboratory of Environmental Functional Materials and Pollution Control, Henan Normal University, Xinxiang 453007, Henan, PR China*

[b] *Key Laboratory of Green Chemical Media & Reactions (Ministry of Education), Xinxiang 453007, Henan, PR China*

[c] *Department of Chemistry, Xinxiang Medical University, Xinxiang, Henan 453003, PR China*

[d] *College of Chemistry, Nankai University, Tianjin 300071, China*

[*] Corresponding authors
E-mail: zhoujgwj@sina.com (J.G. Zhou); Si-MinXu@nankai.edu.cn (S.-M. Xu).

Contents

Removal rate and apparent rate constant

The removal efficiency, η was calculated as eq 1:

$$\eta=\frac{C_0\text{-}C}{C_0} \tag{1}$$

where C_0 is the initial concentration and C is the time-dependent concentration of OFL after irradiation. In addition, since the initial concentration of reactant was low, photodegradation reaction followed the Langmuir-Hinshelwood kinetics model. The apparent rate constant (k_{app}) values were calculated from the plotting of $\ln(C_0/C)$ versus the irradiation time (t) as eq 2:

$$\ln\frac{C_0}{C}=k_{app}t \tag{2}$$

where C_0 is the concentration after stirring for 30 min in the dark and C is the concentration of OFL at time t.

Reactive species analysis

To further understand the photocatalytic mechanism of β-Bi_2O_3@WS_2 core/shell heterostructure composites, suitable sacrificial agents were added to trap active species. Disodium ethylenediamine-tetraacetic acid (EDTA-2Na), 1,4-benzoquinone (BQ) and isopropanol (IPA) was used as scavengers for photogenerated hole (h^+), superoxide radical ($\bullet O_2^-$) and hydroxyl radical (•OH), respectively. The concentration of sacrificial agent was 1 mmol·L^{-1}.

Table S1. The actual Bi and W content in the β-Bi_2O_3@WS_2 composites

Samples	Bi (wt%)	W (wt%)
BO@WS-1	82.96	0.61
BO@WS-2	80.97	2.56
BO@WS-3	77.27	5.21
BO@WS-4	79.35	7.48

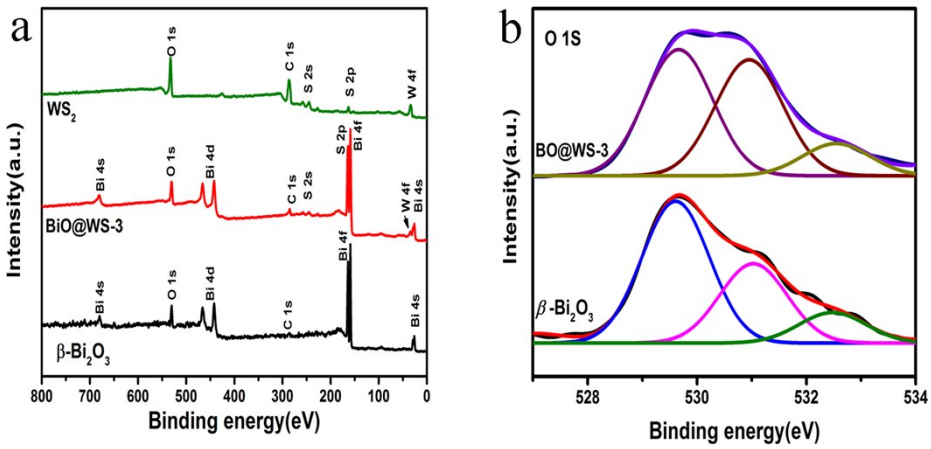

Figure S1. (a) XPS measurement results of full range XPS spectrum for β-Bi_2O_3, E-WS, and BO@WS-3. (b) XPS spectra of O 1s in β-Bi_2O_3, and BO@WS-3.

Figure S2. FE-SEM images of (a) BO@WS-1, (b) BO@WS-2, and (c) BO@WS-4.

BET analysis

The larger specific surface for photocatalyst could provide more active sites, which benefited the adsorption of contaminant and thus facilitated the photocatalytic degradation reaction. Hence, nitrogen adsorption−desorption isotherms and pore size distribution curves of as-prepared samples were displayed in Figure S3. The BET surface areas of the as-prepared β-Bi_2O_3, BO@WS-1, BO@WS-2, BO@WS-3, BO@WS-4 and E-WS was 2.33, 3.65, 4.08, 5.37, 0.29 and 6.53 m^2/g (Table S2), respectively. After the coating of WS_2, the BET surface areas of β-Bi_2O_3@WS_2 composites increased. However, when the WS_2 content was further increased, the surface area of BO@WS-4 sharply decreased because excessive WS_2 nanosheets

tended to aggregate together. The nitrogen isotherms were classified as type IV with a distinct hysteresis loop, suggesting the presence of mesopore. The mesopores were confirmed by the corresponding pore size distribution curves (Figure S3b). As is displayed, β-Bi_2O_3 shows mesopores with peak pore diameter ranging from 30 to 40 nm. E-WS showed the smaller pore volume and average pore size than the others. The specific surface area, pore volume and pore size distribution of different samples are summarized in Table S2. In general, the BO@WS-3 shows larger BET surface area, pore volume and average pore size than β-Bi_2O_3.

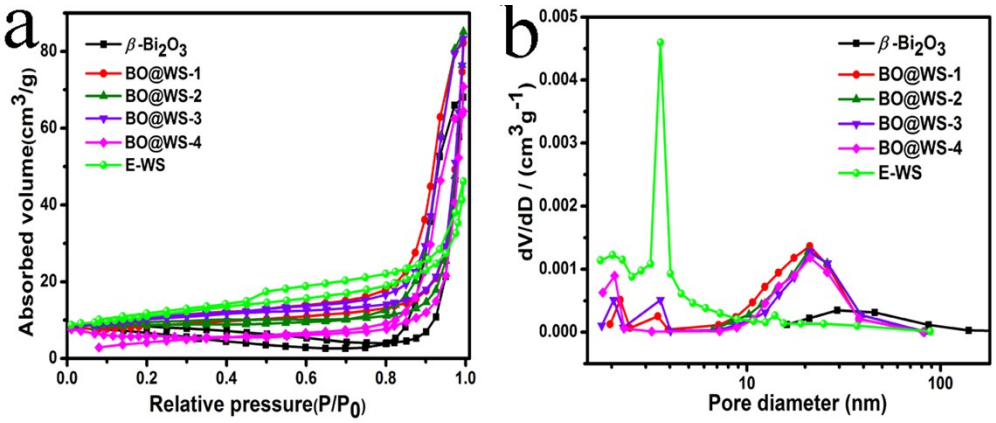

Figure S3. (a) N_2 adsorption–desorption; and (b) the pore size distribution of different samples.

Table S2. Surface areas, pore volumes and diameters for the synthesized samples

sample	specific surface area (m^2/g)	pore volume (cm^3/g)	average pore diameter (nm)
β-Bi_2O_3	2.83	0.0294	9.94
BO@WS-1	3.65	0.0335	20.3
BO@WS-2	4.08	0.0347	24.7
BO@WS-3	5.37	0.0375	22.8
BO@WS-4	0.20	0.0298	20.4
E-WS	6.53	0.0178	8.44

Stability of photocatalyst

The photocatalytic stability and recyclability of the samples are pivotal to practical applications. In order to evaluate the stability of BO@WS-3, five consecutive cycles were performed to test the photocatalytic activity of BO@WS-3 for degradation of OFL under the same conditions. As shown in Figure S4a, the photocatalytic activity of BO@WS-3 was not significantly reduced for OFL degradation, illustrating the stability of BO@WS-3. Furthermore, the XRD patterns of BO@WS-3 (Figure S4b) showed no observable changes before and after the photocatalytic reaction, further indicative of its stability. Therefore, these results confirmed that BO@WS-3 could be used as a promising candidate for practical applications.

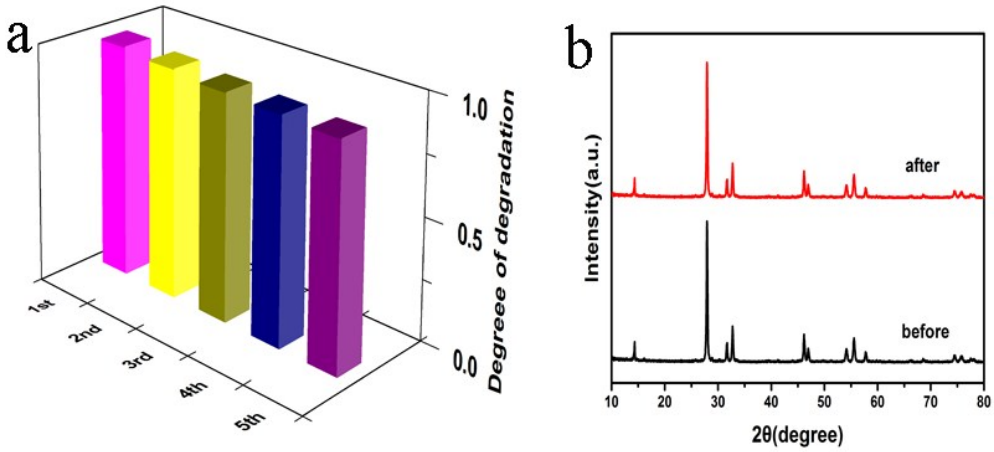

Figure S4. (a) Cyclic runs of BO@WS-3 for the degradation of OFL under visible-light irradiation; (b) XRD patterns of the BO@WS-3 sample before and after five-cycle experiments.

Table S3. Photocatalytic ofloxacin degradation performances of different reaction systems

photocatalyst	light source	c_{OFL} ($mg \cdot L^{-1}$)	reaction time (min)	catalyst amount ($g \cdot L^{-1}$)	rate constant (min^{-1})	reference
mesoporous g-C_3N_4	$\lambda > 290$ nm	4	50	1	0.0460	*Appl. Catal. B: Environ.*, 2018, **227**, 114-122.
P,O-doped g-C_3N_4	$\lambda > 420$ nm	10	80	1	0.0076	*Chem. Eng. J.*, 2019, **374**, 242-253.
B,N-doped TiO_2	solar spectrum	10	240	0.2	0.0238	*Chem. Eng. J.*, 2019, **378**, 122226.
UiO-67/CdS/rGO	$\lambda > 420$ nm	10	90	0.005	0.0101	*Chem. Eng. J.*, 2020, **381**, 122771.
BiOCl/TiO_2	gold halide	200	10	0.15	0.0700	*J. Photochem. Photobiol.*, 2019,

composites	lamp					**378**, 114-124.
$Bi_xO_yCl_2$	halogen lamp	15	120	1	0.0071	*Catal. Sci. Technol.*, 2018, **8**, 4052-4069.
mpg-C_3N_4/CQDs	$\lambda > 420$ nm	8	120	0.5	0.0075	*Dalton Trans.*, 2018, **47**, 1284-1293.
10 wt% MoO_3/Ag/C_3N_4	$\lambda > 420$ nm	20	100	0.02	0.0096	*Chem. Eng. J.*, 10.1016/j.cej.2019.123504.
PCN-222/g-C_3N_4	$\lambda > 420$ nm	20	200	1	0.0048	*Chem. Eng. J.*, 2019, **368**, 165-174.
Bi_2S_3/Bi_2WO_6	$\lambda > 420$ nm	20	180	1	0.0048	*Chem. Eng. J.*, 2018, **354**, 692-705.
Bi_2O_3/TiO_2	solar spectrum	25	120	0.5	0.0077	*Chem. Eng. J.*, 2016, **290**, 45-52.
BO@WS-3	$\lambda > 420$ nm	10	60	1	0.0162	this work

TOC removal efficiency

To further confirm the photocatalytic activity of the BO@WS-3, the decrease of total organic carbon (TOC) was measured to evaluate the extent of mineralization during the photocatalytic degradation of OFL (Figure S5). After 60 min of treatment, the removal efficiency of OFL attained 97.3%, while only 47.2% of TOC removal was observed. The lower mineralization rate in comparison with the corresponding heterogeneous photodegradation rate of OFL could be ascribed to the existence of organic intermediates. Furthermore, 68.5% TOC was attained after 120 min of irradiation, indicating that total mineralization could be further increased with longer irradiation times.

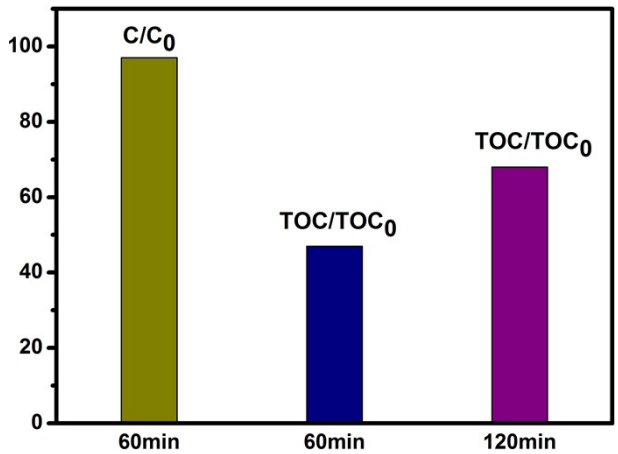

Figure S5. The removal efficiency of OFL and TOC after 60 min, and TOC after 120 min.